

# Plasma conversion of CH<sub>4</sub> followed by post-plasma catalysis for selective C<sub>2</sub>H<sub>4</sub> formation: linking nanosecond pulsed experiments and chemical kinetics models

Eduardo Morais,<sup>1</sup> Marco Scapinello,<sup>2</sup> Gregory Smith,<sup>1</sup> Georgios D. Stefanidis,<sup>2</sup> Annemie Bogaerts<sup>1</sup>

<sup>1</sup> PLASMANT, Department of Chemistry, University of Antwerp, Wilrijk-Antwerp 2610, Belgium

<sup>2</sup> Laboratory for Chemical Technology, Ghent University; Tech Lane Ghent Science Park 125, Ghent, B-9052, Belgium

**Abstract:** Combining non-thermal plasmas and heterogeneous catalysis for gas conversion holds promise for energy efficient CH<sub>4</sub> coupling and enhancing the overall C<sub>2</sub>H<sub>4</sub> yield. In this contribution, we present the results from CH<sub>4</sub> conversion experiments using nanosecond pulsed discharges (NPD) in a coaxial reactor equipped downstream with a Pd catalyst bed for optimal C<sub>2</sub>H<sub>4</sub> formation. We also describe the development of chemical kinetics plasma and surface models to elucidate the underlying chemistry and offer experimental insights in this research.

**Keywords:** Plasma catalysis, nanosecond pulses, CH<sub>4</sub> conversion, selective C<sub>2</sub>H<sub>4</sub> formation.

## 1. Introduction

Although CH<sub>4</sub> prices are decreasing globally due to technological advances and recently discovered natural gas sources, exploration of CH<sub>4</sub> is regarded as problematic as (i) it often occurs at remote sites where transport is difficult and (ii) CH<sub>4</sub> is already released in large amounts as a by-product from coal mining. Therefore, it is desirable to convert CH<sub>4</sub> into more readily transportable and valuable products, such as C<sub>2</sub> olefins.[1] Among these, ethylene (C<sub>2</sub>H<sub>4</sub>) has the highest market value because it is a basic building block for a very broad range of chemicals, including polymers, synthetic fibres, alcohols, and solvents.[2]

Traditional avenues for CH<sub>4</sub> conversion to olefins consist of thermally driven catalytic oxidative or non-oxidative coupling of methane (OCM and NOCM, respectively). Non-oxidative coupling of methane is a generally more selective approach, yielding a smaller range of products with higher added value than the oxidative route. NOCM is also advantageous as it can be carried out in a one-step-process fashion and forgoes oxidants. However, efficient ethylene synthesis via thermal NOMC is a challenging process because, besides this being a highly endothermic and energy-intensive reaction (> 1000 °C), it is usually accompanied by significant amounts of coking which leads to catalyst poisoning and poses hindrance to industrial applications.[2] Thus, electrified alternatives for CH<sub>4</sub> coupling have gained attention in the energy and gas conversion fields.

Employing solar and wind electricity coupled with plasma technology as a “turnkey” strategy is of particular interest because it allows for the thermodynamically unfavourable process of CH<sub>4</sub> splitting to occur via energy-efficient avenues, making use of renewable resources.[3] A range of different types of plasma technologies have been tested in NOCM. While in dielectric barrier discharges (DBDs) C<sub>2</sub>H<sub>6</sub> is formed as the major product (alongside C<sub>3</sub> hydrocarbons), C<sub>2</sub>H<sub>2</sub> and C<sub>(s)</sub> formation dominates in high-energy density or warm plasmas such as microwave (MW), gliding arc (GA) and sparks discharges.[4]–[6] As for C<sub>2</sub>H<sub>4</sub>, selectivity is mildly enhanced in corona discharges, yet the overall yield remains low. The reason for the broad product distribution lies in the different electron density and electron temperature featured in each plasma system,

which in turn determine the operating temperature and consequently, drive the plasma chemistry. Collectively, plasma is not very selective to C<sub>2</sub>H<sub>4</sub> production, unless it can be integrated with a catalytic system suitable for C<sub>2</sub>H<sub>2</sub> hydrogenation to C<sub>2</sub>H<sub>4</sub> in the post-plasma zone.[7] In this context, plasma-assisted heterogeneous catalysis rises as a pioneering strategy to improve the performance of CH<sub>4</sub> conversion, as well as the selectivity towards C<sub>2</sub>H<sub>4</sub>. [6]

In a recent study [8], we have demonstrated that transient plasmas such as nanosecond pulsed discharges (NPD) can be utilised to promote NOCM (coaxial reactor, in the presence of H<sub>2</sub>) with high energy efficiency, producing C<sub>2</sub>H<sub>4</sub> as major product when operating in the 3 – 5 bar pressure range. A zero-dimensional plasma chemical kinetics model was developed to elucidate the effects of gas temperature and pressure on gas conversion and product selectivity, as well as to uncover important reaction pathways and provide an analysis of the dynamics of the heating and cooling mechanisms in the plasma zone.

Aiming to expand the previous work, we have investigated the attachment of a catalyst bed packed with Pd-coated beads downstream from the plasma zone in the NPD experiments in a coaxial reactor (Fig 1a). [7] The purpose of this design was to promote the catalytic hydrogenation of C<sub>2</sub>H<sub>2</sub> (which is the main product in the plasma region) into C<sub>2</sub>H<sub>4</sub> at 1 bar (as shown in Fig. 1).

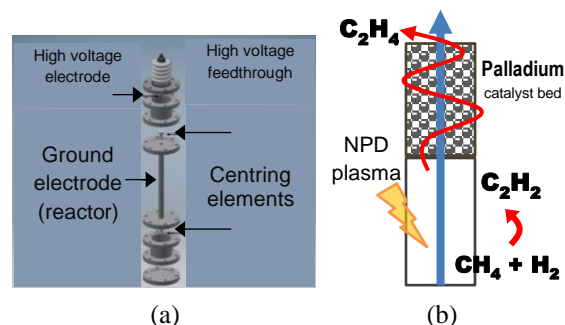


Fig. 1. (a) Coaxial reactor used in the experiments with parts indicated, [7] (b) illustration of the hybrid plasma-catalytic NPD reactor coupled with a Pd bed.

In this contribution, we discuss the performance of this NPD plasma reactor and the activity of this palladium-based catalyst. We also present the results of two chemical

kinetics models to describe (i) the plasma-driven conversion of CH<sub>4</sub> and H<sub>2</sub> into (mostly) C<sub>2</sub>H<sub>2</sub> at 1 bar, and (ii) the hydrogenation of C<sub>2</sub>H<sub>2</sub> into C<sub>2</sub>H<sub>4</sub> over a Pd surface.

## 2. Experimental Setup

The discharge was ignited by a nanosecond pulsed power supply (n-PS) (NPG-18/100k, Megaimpulse Ltd.) which was triggered by a waveform generator (WFG) (33220A, Keysight Technology) at 3 kHz pulse repetition frequency. A high-voltage probe (P6015A Tektronix, 75 MHz bandwidth) and an I/V converter (CT-D-1.0, Magnelab, 200Hz-500MHz bandwidth) were used for the pulse voltage and current measurement, respectively. The coaxial plasma reactor consisted of an inner, copper-based, axial wire (high voltage electrode) and an outer, stainless steel-based, coaxial tube of 10.4 mm internal diameter (ground electrode). The interelectrode distance was 4.2 mm and the length of the reactor was 25 cm. Mass flow controllers (GF40 Series, Brooks Instrument) controlled the feed flow rate of the reactants (100 sccm CH<sub>4</sub> and 100 sccm H<sub>2</sub>; Air Liquide 99.995% purity).

The catalytic bed consists of granulates made from alumina and Pd(NO<sub>3</sub>)<sub>2</sub> which was later calcined to PdO at 300 °C and then reduced to Pd<sup>0</sup> in a H<sub>2</sub> flow prior to use in the NPD experiments. [7] A filter was placed between the plasma and the catalytic region to prevent eventual solid particles from reaching the catalyst.

Analysis of the plasma reactor effluent was performed by an online gas chromatograph (3000 MicroGC, Inficon). H<sub>2</sub>, N<sub>2</sub> and CH<sub>4</sub> were detected by a molesieve column (10 m) with backflush (3 m, Plot U), while for C<sub>2</sub> species a Plot U column (10 m) with backflush (1 m, Plot Q) was used.

## 3. Model description

The zero-dimensional plasma chemical kinetic model was constructed using the ZDPlasKin kinetic solver,[9] which operates by evaluating the continuity differential equation for each chemical species considered in the model, based on species density, stoichiometry and reaction rate. Reactions that do not involve electron collisions use rate coefficients  $k_r$  from literature.  $k_r$  was given within a temperature range and written as a function of gas temperature where such data existed. In the case of electron impact reactions,  $k_r$  was extracted from continuous evaluation of collisional cross sections and the electron energy distribution function (EEDF) via the BOLSIG+ solver, which operates in tandem with ZDPlasKin.

A mixture of CH<sub>4</sub> and H<sub>2</sub> at a 50/50 ratio was adopted as input gas and the species included in the model comprise CH<sub>4</sub> and H<sub>2</sub> molecules in ground and some excited states, C and H atoms, various compounded C<sub>x</sub>H<sub>y</sub> molecules, as well as the corresponding radicals and ions, as shown in Table 1. These species react with each other in many processes leading to an extensive reaction set, comprising 1761 reactions in total. This chemistry was built upon the basis of an earlier publication by PLASMANT, which investigated the utilisation of different plasma sources in CH<sub>4</sub> conversion.[5]

Table 1. Species considered in the plasma (top rows) and surface (bottom row) models.

Stable molecules	Radicals
CH <sub>4</sub> H <sub>2</sub> C <sub>2</sub> H <sub>2</sub> C <sub>2</sub> H <sub>4</sub> C <sub>2</sub> H <sub>6</sub> C <sub>3</sub> H <sub>6</sub> C <sub>3</sub> H <sub>8</sub> C <sub>4</sub> H <sub>10</sub> C <sub>(s)</sub>	H C C <sub>2</sub> C <sub>3</sub> CH <sub>3</sub> CH <sub>2</sub> CH C <sub>2</sub> H C <sub>2</sub> H <sub>3</sub> C <sub>2</sub> H <sub>5</sub> C <sub>3</sub> H <sub>5</sub> C <sub>3</sub> H <sub>7</sub> C <sub>4</sub> H <sub>9</sub>
Ions and electrons	Excited molecules
H <sup>+</sup> H <sub>2</sub> <sup>+</sup> H <sub>3</sub> <sup>+</sup> C <sup>+</sup> C <sub>2</sub> <sup>+</sup> CH <sup>+</sup> CH <sub>2</sub> <sup>+</sup> CH <sub>3</sub> <sup>+</sup> CH <sub>4</sub> <sup>+</sup> CH <sub>5</sub> <sup>+</sup> C <sub>2</sub> H <sup>+</sup> C <sub>2</sub> H <sub>2</sub> <sup>+</sup> C <sub>2</sub> H <sub>3</sub> <sup>+</sup> C <sub>2</sub> H <sub>4</sub> <sup>+</sup> C <sub>2</sub> H <sub>5</sub> <sup>+</sup> C <sub>2</sub> H <sub>6</sub> <sup>+</sup> H <sup>-</sup> CH <sup>-</sup> CH <sub>2</sub> <sup>-</sup> electrons	Vibrational: H <sub>2</sub> (v = 1...14) CH <sub>4</sub> (v = 1...4) Electronic: H <sub>2</sub> <sup>†</sup> CH <sub>4</sub> <sup>†</sup>
Surface kinetics species (*: surface-adsorbed species)	
H <sub>2(g)</sub> CH <sub>4(g)</sub> C <sub>2</sub> H <sub>2(g)</sub> C <sub>2</sub> H <sub>4(g)</sub> C <sub>2</sub> H <sub>6(g)</sub> CH <sub>3(g)</sub> H <sub>(g)</sub> H* CH <sub>3</sub> * CH <sub>2</sub> * CH* C* C <sub>(s)</sub> C <sub>2</sub> H <sub>2</sub> * C <sub>2</sub> H <sub>3</sub> * C <sub>2</sub> H <sub>4</sub> * C <sub>2</sub> H <sub>5</sub> * C <sub>2</sub> H <sub>6</sub> *	

For the surface model, we assembled a series of chemical processes related to adsorption, desorption and surface reactions between H<sub>2</sub>/hydrocarbons and a (111) palladium substrate. The solver evaluates the surface coverage of adsorbates as a function of time at a given temperature. The coverages are dependent on the stoichiometry and rate of adsorption/ desorption of each species. To evaluate the desorption and adsorption rates, the coverage of adsorbates and the partial pressures of gas-phase species are required, alongside the forward and reverse surface reaction rate coefficients. The latter are assessed via harmonic transition state theory using the Eyring-Polanyi equation:

$$k_{TST} = \frac{k_B T}{h} e^{\frac{\Delta S^\ddagger}{R}} e^{-\frac{\Delta H^\ddagger}{RT}} \quad (1)$$

where  $k_B$  is the Boltzmann constant,  $h$  is Planck's constant and  $\Delta S^\ddagger$  and  $\Delta H^\ddagger$  are the entropic and enthalpic barriers to the transition state, respectively. The model is solved in the form of differential equations and each iterative solution requires the coverages and partial pressures which are provided by the solution of the model at steady state in the previous timestep.

## 4. Results and discussion

To resolve the effects of plasma conversion and catalysis, the performance of the NPD reactor without the catalyst attachment was assessed first. The conversion and selectivity figures derived from GC measurements are as follows: 32% CH<sub>4</sub> conversion, 52% C<sub>2</sub>H<sub>2</sub>, 19% C<sub>2</sub>H<sub>4</sub> and 6% C<sub>2</sub>H<sub>6</sub> selectivity. Both conversion and C<sub>2</sub> selectivity remained very close to those previously observed in a coaxial reactor [8]. As C<sub>2</sub>H<sub>2</sub> is most stable at higher temperatures, this selectivity trend highlights the high temperatures predicted by the model in the plasma zone (> 1400 °C). These results corroborate that C<sub>2</sub>H<sub>2</sub> is the main product at 1 bar using NPD.

In further experiments, the catalytic unit was attached to the exhaust of the plasma reactor to hydrogenate the C<sub>2</sub>H<sub>2</sub> formed in the plasma zone into C<sub>2</sub>H<sub>4</sub> (using the H<sub>2</sub> in the gas feed). [7] The results (Fig. 2) show this was successfully achieved, with C<sub>2</sub>H<sub>4</sub> being the new main product (63%), followed by C<sub>2</sub>H<sub>6</sub> (12%) and C<sub>2</sub>H<sub>2</sub> (4%).

With hot gas exiting the plasma region, the temperature of the catalyst reached  $\sim 600$  K and no additional heating was required. When the catalyst was tested in the absence of the thermal activation provided by the plasma, no catalytic activity was registered (even when  $C_2H_2$  and  $H_2$  were used as reactants).

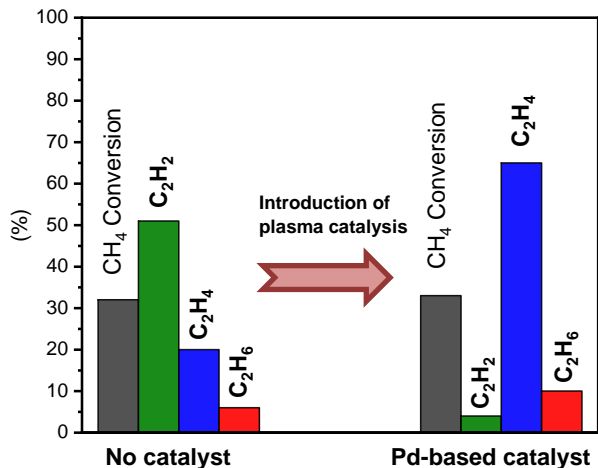


Fig. 2. Conversion and  $C_2$  selectivity results before and after the introduction of the Pd-based catalyst. [7]

The plasma chemical kinetic model was used to investigate the plasma characteristics and the behaviour of physical parameters, such as reduced electric field ( $E/N$ ), electron and gas temperature during the NPD. The response of the reduced electric field (and in turn of the gas temperature) to the power pulses is plotted in Fig. 3. Akin to the power discharges, the  $E/N$  profile (and electron temperature) exhibits pulsed behaviour, and the peaks are coincidental in time with the power pulses. This is expected as the model computes the electric field from the power input, and in turn the electric field is supplied to BOLSIG+ for EEDF calculations and electron temperature. The latter determine the energy of electrons in the plasma zone, which will initiate chemical reactions with the incoming  $CH_4$  and  $H_2$  molecules in the gas flow.

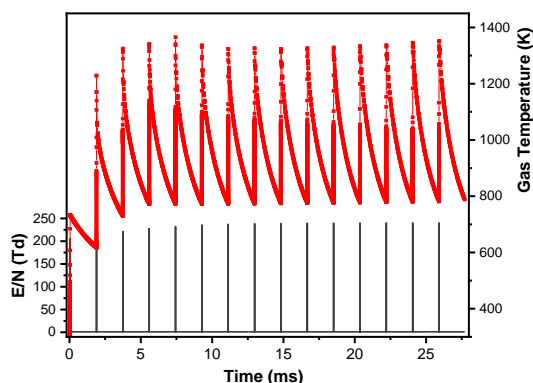


Fig. 3. Simulated temporal profiles of reduced electric field  $E/N$  (bottom) and gas temperature (top). It is noteworthy that both profiles exhibit pulsed behaviour and the peaks are coincident with each other and with the NPD.

The gas temperature profile also exhibits pulsed behaviour. While heating (leading to temperature peaks) occurs for  $\sim 120$  ns after each power pulse, cooling begins subsequently and is a much slower process (resembling that of an exponential decay) as it takes place on the ms scale ( $\sim 1.2$  ms) during the afterglow until the next pulse. The calculated gas temperatures ( $T_{\text{gas}} = 1400 - 800$  K, with an average of 1100 K) are starkly lower than the calculated electron temperatures ( $T_e = 39000 - 51000$  K or 3.6 - 4.2 eV), clearly indicating that the system operates in a non-thermal plasma regime in all cases.

This model was also used to calculate time-dependent concentrations of species during the NPD and in the afterglows. The densities of electrons, ions and radicals peak with the power pulses and drop to much lower values in the afterglow. The electron density reaches a maximum of  $\sim 10^{16}$   $\text{cm}^{-3}$  at the top of each pulse (when electron impact reactions dominate the plasma chemistry) and plummets to  $\sim 5.0 \times 10^8$   $\text{cm}^{-3}$  in the afterglows (in between the pulses), slowing down or halting electron impact processes, as recombination reactions become more important.  $CH_4$  and  $H_2$  are chiefly decomposed through electron impact reactions during the power discharges, and reformed otherwise via the very efficient recombination channels of  $CH_3 + H$  and  $H + H$ , respectively. Concomitantly, other recombination reactions lead to the formation of higher hydrocarbons such as  $C_2H_2$  (main product) and  $C_2H_4$ . Overall, excellent agreement was observed between modelled and experimental conversion and selectivity figures.

Moreover, reaction pathway analyses were extracted from the model (Fig.4). Unsurprisingly, H radicals were found to be the most populous plasma species and they participate in all (de)hydrogenation reactions, which are the dominant recombination processes leading to  $C_2H_2$  being the main product at 1 bar.[10]

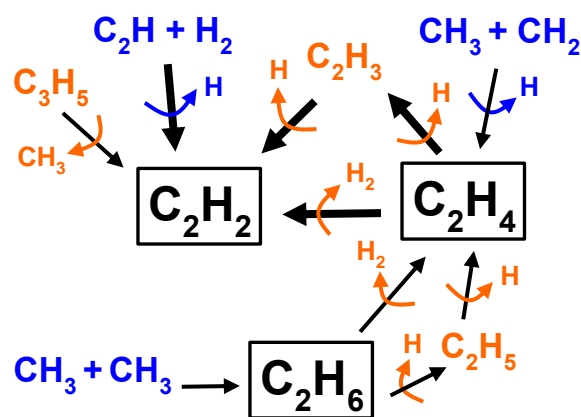


Fig. 4. The network of species and reactions involved in  $C_2$  selectivity equilibrium in steady state at 1 bar. Thicker arrows in the diagram indicate important reactions, blue arrows indicate recombination reactions and orange arrows indicate decomposition reactions.

The surface chemical kinetics model was used to describe the interaction between the gaseous species present in the plasma reactor's effluent and the surface of the palladium catalyst. Using the results from the experiments and plasma kinetic model as inputs for the partial pressures in this study and 600 K as constant temperature, it is clear that three main gaseous species come in contact with the Pd-coated element:  $\text{CH}_4(\text{g})$ ,  $\text{H}_2(\text{g})$  and  $\text{C}_2\text{H}_2(\text{g})$ . As these molecules traverse the catalytic region, they adsorb onto the palladium surface and have three different reactive pathways, as shown in Fig.5.

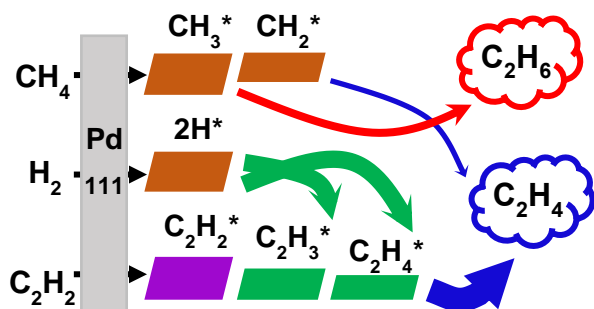


Fig. 5. Flow diagram showing the main reaction pathways in the catalytic hydrogenation of  $\text{C}_2\text{H}_2$  into  $\text{C}_2\text{H}_4$  over a Pd (111) surface. The \* notation signals adsorbed species and thicker arrow lines indicate higher reaction rates.

The  $\text{CH}_4$  molecules undergo immediate surface stepwise dehydrogenation to form adsorbed  $\text{CH}_3$  and  $\text{CH}_2$  (and H). A fraction of the  $\text{CH}_3$  species recombine to produce adsorbed  $\text{C}_2\text{H}_6$ , which will eventually be desorbed into the gas phase and detected in the experiments. In turn, further  $\text{CH}_3$  dehydrogenation forms  $\text{CH}_2$  which is converted into  $\text{C}_2\text{H}_4$  via a surface recombination reaction. The adsorbed  $\text{H}_2$  molecule is very efficiently split into two reactive H species which initially remain attached onto the palladium surface. Subsequently, these H species will enter the channel of stepwise  $\text{C}_2\text{H}_2$  hydrogenation – as they encounter adsorbed  $\text{C}_2\text{H}_2$  species, creating  $\text{C}_2\text{H}_3$  and  $\text{C}_2\text{H}_4$  on the catalyst surface. In the last step,  $\text{C}_2\text{H}_4$  desorbs from the palladium substrate into the gas phase, thus becoming the major product of this process with an overall selectivity of  $\sim 70\%$ . Besides uncovering these reaction mechanisms, this model can also be used to tune the selectivity of the process to different hydrocarbons of interest, or to identify other suitable catalytic materials.

## 5. Conclusions

In this contribution, a NPD has been investigated for methane conversion in a coaxial reactor, which was coupled to a catalytic unit for downstream hydrogenation of acetylene, which was found to be the main product of the plasma-driven reaction. As hot gas travelled from the plasma region, the catalyst was thermally activated, promoting  $\text{C}_2\text{H}_2$  hydrogenation into  $\text{C}_2\text{H}_4$  (the desired final product) over a palladium surface.

The plasma kinetics were successfully described with a chemical kinetics model which showed very good alignment for  $\text{CH}_4$  conversion and product selectivity, signalling that the gas-phase kinetic dynamics occurring in the reactor are comparable to those included in the model. The simulation results highlight pulsed behaviour in all the physical parameters, such as electric field, gas temperature and electron energy, and the species densities also exhibit pulsed profiles. A reaction pathway analysis demonstrates that at 1 bar ( $\sim 1200$  K)  $\text{C}_2\text{H}_2$  is chiefly produced via consecutive dehydrogenations from  $\text{C}_2\text{H}_6$  (the first  $\text{C}_2$  hydrocarbon formed in the plasma zone) passing through  $\text{C}_2\text{H}_4$ , which is the second main product in the NOCM (in the absence of downstream catalysis).

The surface kinetic model revealed the desired  $\text{C}_2\text{H}_4$  final product is indeed majorly formed through hydrogenation of  $\text{C}_2\text{H}_2$  with H species (from  $\text{H}_2$  splitting) on a Pd (111) surface, but also via  $\text{CH}_2 + \text{CH}_2$  surface recombination reactions (to a lesser extent). The same mechanism is valid for adsorbed  $\text{CH}_3$  species which lead to formation of  $\text{C}_2\text{H}_6$  (second overall product). Both  $\text{CH}_3$  and  $\text{CH}_2$  originate from dehydrogenation of adsorbed  $\text{CH}_4$  abundantly present in the gas effluent of the plasma reactor.

## 6. Acknowledgements

We gratefully acknowledge the financial support by the Flemish Government through the Moonshot cSBO project “Power-to-Olefins” (P2O; HBC.2020.2620).

## 7. References

- [1] I. Amghizar, L. A. Vandewalle, K. M. Van Geem, and G. B. Marin, *Engineering*, **3**, 171-178 (2017).
- [2] Y. Engelmann, P. Mehta, E. C. Neyts, W. F. Schneider, and A. Bogaerts, *ACS Sustain. Chem. Eng.*, **8**, 6043-6054 (2020).
- [3] A. Bogaerts and E. C. Neyts, *ACS Energy Letters*, **3**, 1013-1027 (2018).
- [4] E. Delikonstantis, M. Scapinello, O. Geenhoven, and G. D. Stefanidis, *Chem. Eng. J.*, **380**, 122477 (2019).
- [5] S. Heijkers, M. Aghaei, and A. Bogaerts, *J. Phys. Chem. C*, **124**, 7016-7030 (2020).
- [6] N. García-Moncada, G. van Rooij, T. Cents, and L. Lefferts, *Catal. Today*, **369**, 210-220 (2021).
- [7] E. Delikonstantis, M. Scapinello, and G. D. Stefanidis, *Fuel Process. Technol.*, **176**, 33-42 (2018).
- [8] E. Morais, E. Delikonstantis, M. Scapinello, G. Smith, G. D. Stefanidis and A. Bogaerts, *Chem. Eng. J.*, <submitted> (2022).
- [9] L. Pancheshnyi, S. Eismann, B. Hagelaar, and G. Pitchford, <user\_manual> <http://www.laplace.univ-tlse.fr>. (2008).
- [10] M. Scapinello, E. Delikonstantis, and G. D. Stefanidis, *Chem. Eng. J.*, **360**, 64-74 (2019).